

Published in final edited form as:

*Nat Med.* 2014 August ; 20(8): 942–947. doi:10.1038/nm.3614.

## A Gpr120 Selective Agonist Improves Insulin Resistance and Chronic Inflammation

Da Young Oh<sup>1,\*</sup>, Evelyn Walenta<sup>1</sup>, Taro E. Akiyama<sup>2</sup>, William S. Lagakos<sup>1</sup>, Denise Lackey<sup>1</sup>, Ariane R. Pessentheiner<sup>1,3</sup>, Roman Sasik<sup>1</sup>, Nasun Hah<sup>4</sup>, Tyler J. Chi<sup>1</sup>, Jason M. Cox<sup>2</sup>, Mary Ann Powels<sup>2</sup>, Jerry Di Salvo<sup>2</sup>, Christopher Sinz<sup>2</sup>, Steven M. Watkins<sup>5</sup>, Aaron M. Armando<sup>6</sup>, Heekyung Chung<sup>1</sup>, Ronald M. Evans<sup>4,7</sup>, Oswald Quehenberger<sup>1,6</sup>, Joanne McNelis<sup>1</sup>, Juliane G. Bogner-Strauss<sup>3</sup>, and Jerrold M. Olefsky<sup>1,\*</sup>

<sup>1</sup> Division of Endocrinology and Metabolism, Department of Medicine, University of California, San Diego, La Jolla, CA 92093, USA

<sup>2</sup> Merck Research Laboratories, Kenilworth, NJ 07033, USA

<sup>3</sup> Institute of Biochemistry, Graz University of Technology, Petersgasse 12 A-8010 Graz, Austria

<sup>4</sup> Gene Expression Laboratory, Salk Institute for Biological Studies, La Jolla, CA 92037, USA

<sup>5</sup> Lipomics Technologies, Inc., West Sacramento, CA 95691, USA

<sup>6</sup> Department of Pharmacology, University of California, San Diego, La Jolla, CA 92093, USA

<sup>7</sup> Howard Hughes Medical Institute, Salk Institute for Biological Studies, La Jolla, CA 92037, USA

It is well known that the omega-3 fatty acids ( $\omega$ 3-FAs) contained in fish oils can exert potent anti-inflammatory effects <sup>1-4</sup>.  $\omega$ 3-FAs are commonly consumed as fish products, dietary supplements, and pharmaceuticals and a number of health benefits have been ascribed to them, including a reduction in plasma triglyceride levels, amelioration of atherosclerosis, and increased insulin sensitivity <sup>5-7</sup>. We reported that Gpr120 is the functional receptor/sensor for these fatty acids and that  $\omega$ 3-FAs produce robust anti-inflammatory, insulin sensitizing effects, both *in vivo* and *in vitro* in a Gpr120-dependent manner <sup>8</sup>. Indeed, human genetic variants in the *Gpr120* gene had been described which predispose to obesity and diabetes <sup>9</sup>. However, the amount of fish oils which would have to be consumed to sustain chronic agonism of Gpr120 is too high to be practical, and, thus, a high affinity, small molecule Gpr120 agonist would be of potential clinical benefit. Accordingly, Gpr120 is a widely studied drug discovery target within the pharmaceutical industry. Gpr40 is another lipid sensing GPCR <sup>10</sup>, and it has been difficult to identify compounds with a high degree of

\* To whom correspondence should be addressed; Da Young Oh, PhD (dayoungoh@ucsd.edu) and Jerrold M. Olefsky, MD (jolefsky@ucsd.edu) Division of Endocrinology & Metabolism, Department of Medicine, University of California, San Diego, 9500 Gilman Drive, La Jolla, CA, 92093, USA. Phone: 858-822-6647 Fax: 858-534-6653.

### Author contributions

D.Y.O. designed the studies and performed the experiments; R.S. carried out RNA-seq data analysis; D.Y.O. and J.M.O. analyzed, interpreted data, and co-wrote the manuscript. All other authors performed experiments and contributed to discussions. This work was supported by grants to J.M.O. and D.Y.O. as detailed above.

### Competing financial interests

The authors declare no competing financial interests.

selectivity for Gpr120 vs. Gpr40<sup>11</sup>. Here we report that a high affinity, selective, small molecule Gpr120 agonist (cpdA), exerts potent anti-inflammatory effects on macrophages *in vitro*, and in obese mice *in vivo*. Gpr120 agonist treatment of high fat diet (HFD)/obese mice causes improved glucose tolerance, decreased hyperinsulinemia, increased insulin sensitivity and decreased hepatic steatosis. This suggests that Gpr120 agonists could become new insulin sensitizing drugs for the treatment of Type 2 diabetes and other human insulin resistant states in the future.

Gpr120 and Gpr40 are 2 lipid sensing G protein-coupled receptors (GPCRs)<sup>10,12</sup>, but despite limited homology between these two polyunsaturated fatty acid (PUFA) receptors, identification of ligands that are highly selective for Gpr120 over Gpr40 has been challenging<sup>11,13-15</sup>. We have generated a small molecule Gpr120 agonist, compound A (cpdA) (Fig. 1a), and have examined its selectivity for Gpr120 compared to Gpr40 using a Ca<sup>2+</sup> FLIPR assay (Fig. 1b). CpdA was fully selective for Gpr120 (logEC50 (M) = -7.62 ± 0.11) with negligible activity towards Gpr40 (Fig. 1b). Gpr120 couples to Gαq/11-initiated signal transduction pathways, and, as such, we assessed the activity of cpdA in an inositol-1, 4, 5-triphosphate (IP<sub>3</sub>) production assay, employing HEK 293 cells that stably express human or mouse Gpr120. The Gpr120 agonist produced concentration dependent increases in IP<sub>3</sub> production from both human and mouse Gpr120 expressing cells (Fig. 1c). In addition to promoting signaling via Gαq/11, Gpr120 also directly couples to β-arrestin-2<sup>8,14</sup>. Therefore, we examined the potency of cpdA in a β-arrestin-2 recruitment assay (Fig. 1d). CpdA led to a concentration-dependent response to recruit β-arrestin-2 in both human and mouse Gpr120 expressing cells, with EC50s of ~0.35 μM (Fig. 1d). Since Gpr120 is a Gαq/11-coupled receptor, it stimulates both PKC and MAP kinase, and both of these biologic effects can be detected in an SRE-driven reporter system<sup>8</sup>. HEK293 cells were transiently transfected with constructs for mouse Gpr120 along with a serum response element-luciferase promoter/reporter (SRE-luc). The Gpr120 SRE-luc reporter cells were treated with docosahexaenoic acid (DHA) and cpdA. Gpr120 stimulation by cpdA was ~50 fold more potent than DHA (Fig. 1e). DHA and cpdA were used at 100 μM and 10 μM in all subsequent studies to achieve maximal effects.

In our previous studies<sup>8</sup>, we showed that Gpr120 stimulation mediated anti-inflammatory responses in macrophages. To link these observations to the cpdA compound, we evaluated the effect of DHA and cpdA on NFκB-driven reporter genes in WT and Gpr120 KO primary macrophages. DHA and cpdA decreased LPS-induced NFκB-reporter gene activity in WT, but not in Gpr120 KO primary macrophages (Fig. 1f). To examine Gpr120-mediated anti-inflammatory properties in a more physiologic context, we treated primary macrophages from WT and Gpr120 KO mice with DHA or cpdA for 1 hr, followed by LPS stimulation. DHA and cpdA strongly and comparably inhibited LPS-induced phosphorylation of Tak1, Iκkβ, and Jnk and blocked IκB degradation (Fig. 1g). LPS-mediated cytokine secretion and inflammatory gene expression were also inhibited in WT, but not in Gpr120 KO primary macrophages (Supplemental Fig. 1a and b).

Next, we determined whether the synthetic Gpr120 agonist could produce beneficial metabolic effects *in vivo*. WT and Gpr120 KO mice were placed on 60% HFD for 15 weeks. At this point, separate groups of 10 mice each were treated for an additional 5 weeks with

60% HFD alone, or HFD containing 30 mg kg<sup>-1</sup> cpdA. The 5 weeks treatment time point was most effective at improving glucose tolerance and lowering insulin concentration (Supplemental Fig. 2). Figure 2 shows that treatment with cpdA led to markedly improved glucose tolerance (Fig. 2a), insulin tolerance (Fig. 2b), and decreased insulin secretion compared to HFD (Fig. 2c) in WT, but not in Gpr120 KO mice, with no change in body weight (Supplemental Fig. 3). These metabolic effects of cpdA treatment were comparable to dietary  $\omega$ 3-FAs supplementation (Supplemental Fig. 4). Importantly, during hyperinsulinemic, euglycemic clamp studies, we found that the cpdA diet caused improved insulin sensitivity with increased glucose infusion rates (GIR), enhanced insulin stimulated-glucose disposal rate (IS-GDR), along with a marked increase in the ability of insulin to suppress hepatic glucose production (HGP) only in WT mice (Fig. 2d). This demonstrates the *in vivo* effects of the Gpr120 agonist to produce systemic insulin sensitivity by enhancing muscle and liver insulin action. In addition to improving hepatic insulin sensitivity, cpdA treatment had beneficial effects on hepatic lipid metabolism, causing decreased hepatic steatosis, decreased liver triglycerides, and DAGs, along with reduced saturated free fatty acid content (Supplemental Fig. 5). In contrast, cpdA administration was without effect to reduce hepatic lipid levels in the Gpr120 KO mice.

Gpr120 can be expressed in enteroendocrine L cells and earlier studies on Gpr120 have focused on its potential ability to stimulate Glp-1 secretion<sup>12</sup>. Therefore, we measured the total and active form of Glp-1 during oral glucose challenge in HFD mice with or without cpdA treatment (Supplemental Fig. 6a). The results demonstrated that Gpr120 activation had no effect to stimulate Glp-1 secretion at 15 min after oral glucose challenge (Supplemental Fig. 6a). Others have also shown a lack of effect of Gpr120 stimulation on Glp-1 secretion<sup>16,17</sup>. We next measured glucose-stimulated insulin secretion (GSIS) in isolated islets from WT and Gpr120 KO mice (Supplemental Fig. 6b) and in the mouse  $\beta$  cell line, MIN6 cells (Supplemental Fig. 6c). CpdA had a slight, but not statistically significant, effect to increase GSIS in WT islets, but was without effect in Gpr120 KO islets. DHA treatment had a stronger effect to increase GSIS, which was comparable in both WT and Gpr120 KO islets (Supplemental Fig. 6b and 6c), showing that this effect of DHA was Gpr120-independent, but Gpr40-mediated as previously reported<sup>10,18</sup>. This is also consistent with the *in vivo* GTT results showing slightly higher insulin levels and lower glucose levels in FOD compared to cpdA treated WT mice (Supplemental Fig. 4). Furthermore, a recent paper by Stone et al.<sup>18</sup> showed that Gpr120 is preferentially expressed in mouse islet delta cells and not detected in  $\beta$  cells, and that Gpr120 activation inhibits glucose-induced somatostatin secretion. Therefore, the slight effect of the Gpr120 agonist on GSIS in isolate islets is most likely an indirect effect from inhibition of somatostatin secretion. This interpretation is fully consistent with our results showing that cpdA has no effect on GSIS in MIN6 cells.

We performed acute insulin response studies by measuring Akt phosphorylation in muscle and liver following an injection of insulin into HFD WT or Gpr120 KO mice. Fully consistent with the *in vivo* glucose clamp studies, this biochemical measure of muscle and hepatic insulin signaling was increased with cpdA treatment in WT, but not in Gpr120 KO

mice (Fig. 2e). Taken together, these results show that the Gpr120 agonist leads to increased systemic insulin sensitivity *in vivo*.

Gpr120 stimulation by  $\omega$ 3-FAs decreases adipose tissue macrophage (ATM) infiltration and reduces inflammatory gene expression<sup>8</sup>. Consistent with this, we observed that cpdA treatment blocked chemotaxis of WT macrophage induced by adipocyte condition medium (CM) as effectively as DHA, but both were without effect in Gpr120 KO macrophages (Fig. 3a). To determine if these *in vitro* chemotaxis results translated to the *in vivo* situation, we directly measured macrophage migration into adipose tissue using an *in vivo* macrophage tracking technique. With this approach, circulating monocytes were obtained from WT donor mice and labeled with fluorescent PKH26 dye *ex vivo*. The labeled monocytes were then injected into recipient HFD WT and Gpr120 KO mice with or without dietary  $\omega$ 3-FAs supplementation or HFD+cpdA treatment. As seen in Figure 3b, there was a substantial decrease in labeled ATM appearance in both  $\omega$ 3-FA and cpdA treated WT mice, with no effect in Gpr120 KO mice. These data were even more revealing when we examined the subpopulations of labeled macrophages between the groups. Thus, ATMs expressing Cd11c are M1-like and proinflammatory (ATM1) compared to M2-like Cd11c negative ATMs (ATM2), which are non-inflammatory. With this analysis, there is an even greater decrease in the number of recruited Cd11c positive ATMs. At the same time, there is an increase in the Cd11c negative ATM population in the cpdA treated WT mice, with no effect in Gpr120 KO mice (Fig. 3b). This shows that cpdA led to reduced monocyte migration with less M1-like Cd11c positive ATMs, and that the labeled monocytes that do become ATMs, favor the M2-like Cd11c negative state. Along with *in vivo* migration results, we also found reduced ATM content by immunohistochemistry (F4/80 staining) in adipose tissue sections from HFD+cpdA treated compared to HFD mice (Fig. 3c). This was accompanied by decreased Cd11c positive ATMs, and increased Cd11c negative ATMs (Fig. 3d and Supplemental Fig. 7a) by FACS analysis. As before, all of these effects were observed in WT, but not in Gpr120 KO mice.

While macrophages are one of the critical immune cells mediating HFD-induced inflammation, recent studies show that other immune cell type, such as T cells and B cells, can contribute to adipose tissue inflammation<sup>19,20</sup>. In particular, Foxp3+ regulatory T (Treg) cells<sup>19</sup> and regulatory B (Breg) cells<sup>20</sup> suppress inflammation in adipose tissue and can secrete IL-10 (Fig. 3e). Therefore, we measured Treg and Breg cells in HFD WT and Gpr120 KO mice with or without cpdA treatment and found increased Treg and Breg cells in adipose tissue from cpdA treated WT mice, but not in Gpr120 KO mice (Supplemental Fig. 7b and c). Taken together, ratio of proinflammatory M1-like ATMs to anti-inflammatory M2-like ATMs+Tregs is markedly decreased with cpdA treatment and this ability of Gpr120 agonism to boost adipose tissue Treg levels may represent an additional therapeutic effect.

We also found decreased expression of a number of proinflammatory genes in epididymal adipose tissue, such as *Tnf- $\alpha$* , *Il6*, *Mcp1*, and *Il1 $\beta$*  (Fig. 3e upper row). At the same time, an increase in anti-inflammatory gene expression, such as *Il-10*, *Clec7a*, *Mgl1*, *Ym1* was observed (Fig. 3e lower row). Interestingly, adipose tissue levels of the proinflammatory arachidonic acid metabolites, leukotriene B4 (LTB4), prostaglandin E2 (PGE2), 5-

hydroxyeicosatetraenoic acid (5-HETE), and leukotriene A4 (LTA4) were also inhibited by both  $\omega$ 3-FA and cpdA treatment (Supplemental Fig. 8). Indicative of systemic inflammation, circulating cytokine levels are elevated in obesity, and as seen in Figure 3f. Inflammatory cytokine levels were markedly reduced in HFD+cpdA treated HFD WT mice but not in HFD Gpr120 KO mice (Fig. 3f). To directly link these observations to inflammatory transcriptional output, we performed RNA-seq analyses in primary macrophages from WT and Gpr120 KO mice. As illustrated in Supplemental Figure 9a, pretreatment of macrophages with DHA or cpdA inhibited LPS-stimulated inflammatory gene expression. Information clustering results revealed that highly significant biological processes (Bonferroni  $p$ -value  $< 0.01$ ) in LPS-stimulated macrophages pretreated with DHA (Supplemental Fig. 9b) or cpdA (Supplemental Fig. 9c) included several inflammation related pathways.

It is known that nitric oxide (NO) can attenuate insulin signaling through nitrosylation of insulin signaling molecules, including Akt<sup>21</sup>. Tissue NO levels represent the balance between iNos and Arginase activity. *iNos* expression was induced in adipose tissue from both WT and Gpr120 KO mice by HFD, and this effect was reduced by cpdA treatment in WT but not Gpr120 KO mice. HFD also led to increased *Arginase* expression, and this increase was enhanced in WT, but not Gpr120 KO mice, with cpdA treatment. Thus, the iNos/Arginase ratio was markedly reduced in WT adipose tissue by HFD+cpdA compared to HFD (Fig. 4a). As would be predicted from these gene expression changes, levels of adipose tissue NO<sub>2</sub>, a stable breakdown product of NO, were reduced ~60% in HFD+cpdA treated WT mice (Fig. 4b). This decrease was almost completely abrogated in Gpr120 KO mice. Consistent with these changes in NO levels, nitrosylation of Akt, was increased on HFD in both WT and Gpr120 KO adipose tissue and this was reduced by HFD+cpdA treatment only in WT adipose tissue (Fig. 4c). Concomitant with this, insulin-stimulated Akt phosphorylation was greater in adipose tissue from HFD+cpdA treated WT mice compared to HFD (Fig. 4d).

To further examine the effect of cpdA on insulin signaling, we isolated primary adipocytes from WT and Gpr120 KO mice for glucose uptake analyses. Ligand-stimulation of Gpr120 led to a modest increase in glucose uptake in primary WT adipocytes, but was without effect in Gpr120 KO adipocytes (Fig. 4e). As previously described for  $\omega$ 3-FAs, Gpr120 agonist-mediated glucose uptake was dependent on G $\alpha$ q/11 signaling and independent of the  $\beta$ -arrestin-2 pathway (Supplemental Fig. 10; <sup>8</sup>).

Recently, the  $\omega$ 3-FA sensing GPCR, Gpr120, has received increasing interest as a therapeutic target for the treatment of both metabolic and inflammatory diseases. Knockout experiments in cells and mice, as well as human genetic studies are consistent with the view that Gpr120 plays an important role in anti-inflammation and insulin sensitization<sup>8,9,12</sup>. Despite this interest, further validation of Gpr120 as a therapeutic target has been hindered by the lack of available small molecule agonists. In our current work, we have used a novel small molecule agonist for Gpr120, cpdA, to explore the pharmacology and function of Gpr120 *in vitro* and *in vivo*. Comparison of cpdA with  $\omega$ 3-FAs clearly demonstrated that this Gpr120 agonist is a selective, potent activator of both human and mouse Gpr120. Most importantly, treatment with this compound *in vitro* and *in vivo*, caused anti-inflammatory,

insulin sensitizing effects, comparable to  $\omega$ 3-FA administration. Taken together, Gpr120 agonists could become future insulin sensitizing agents for the treatment of Type 2 diabetes and other human insulin resistant states.

## Online Methods

### Chemicals and reagents

CpdA was provided from Merck & Co., Inc. (Whitehouse Station, NJ) and DHA was from Cayman chemical (Ann Arbor, MI). All other chemicals were purchased from Sigma unless mentioned otherwise.

### Animal care and use

Male C57Bl/6 WT or Gpr120 KO littermates were fed a normal chow (13.5% fat; LabDiet) or high-fat diet (60% fat; Research Diet) *ad libitum* for 15-20 weeks from 8 weeks of age. Gpr120 KO mice and WT littermates were initially provided by Taconic Inc. (Hudson, NY) and bred further in house, backcrossing with C57Bl/6J mice for > 10 generations. After 15 weeks on HFD, WT and Gpr120 KO mice were switched to an isocaloric HFD supplemented with  $\omega$ 3-FA concentrate<sup>8</sup> or 30 mg kg<sup>-1</sup> cpdA and fed for 5 weeks. Mice received fresh diet every 3rd day, and food consumption and body weight were monitored. Animals were housed in a specific pathogen-free facility and given free access to food and water. All procedures were approved by the University of California San Diego animal care and use committee. *In vivo* metabolic studies were performed as described previously<sup>8</sup>.

### Metabolic studies

We performed GTT, ITT, and hyperinsulinemic euglycemic clamp studies as described<sup>8,22</sup>.

### Acute insulin response

WT and Gpr120 KO mice on HFD or HFD+cpdA were injected with insulin (0.35 U kg<sup>-1</sup>) after 6 hr fast into the inferior vena cava. Tissue species were harvested as described<sup>23</sup>, at the indicated time points and flash frozen in liquid N<sub>2</sub>. We prepared lysates and ran Western blots according to standard protocols.

### Western blotting and gene expression analyses

Western blotting and quantitative PCR (qPCR) were performed as previously described<sup>8,22</sup>. All antibodies are from Cell Signaling Technology.

### SVCs isolation, and FACS analysis

SVC isolation and FACS analyses were performed as previously described<sup>24</sup>. SVCs were incubated with Fc Block (BD Biosciences) for 20 min at 4 °C before staining with fluorescently labeled primary antibodies or control IgGs for 30 min at 4 °C. We used Aqua L-D (Invitrogen) to exclude dead cells. The antibodies used were anti-F4/80-APC (BM8, AbD Serotec), Cd11b-FITC (M1/70, BD Biosciences), Cd11c-PE (HL-3, BD Biosciences), Cd4 (RM4-5, BD Biosciences), Cd19 (MB19-1, eBioscience), Cd22.2 (CY34.1, BD Biosciences), Cd25 (PC61, eBioscience), Cd45R-APC-Cy7 (BD Biosciences), Foxp3

(FJK-16s, eBioscience). Unstained, single stained, and fluorescence minus one controls were used for setting compensation and gates.

### **Immunohistochemistry**

Liver was fixed and embedded in paraffin and sectioned for H&E staining.

### ***In vitro* chemotaxis assay**

*In vitro* chemotaxis assay was performed as previously described <sup>8</sup>.

### ***In vivo* macrophage tracking**

*In vivo* macrophage tracking was performed as previously described <sup>25</sup>. Briefly, blood leukocytes from C57BL/6 WT mice were subjected to red blood cell lysis and monocyte subsets were enriched with EasySep® mouse monocyte enrichment kit (STEMCELL tech, Vancouver, BC) following the manufacture's instructions. Isolated monocytes ( $2 \times 10^6$  to  $5 \times 10^6$ ) were washed once in serum-free medium (RPMI-1640) and suspended in 2 ml of Diluent solution C (included in the PKH26 labeling kit). Two ml of PKH26 (Sigma Chemical Co. St Louis, MO) at  $2 \times 10^{-3}$  M in Diluent C was added and mixed, and the cells were incubated for 10 min at room temperature in the dark. The staining reaction was stopped by addition of an equal volume (2 ml) of medium supplemented with 10% FBS. The mixture was centrifuged and the cells were washed once and resuspended in serum containing medium. Subsequent to labeling with PKH26, the monocytes were counted and  $\sim 0.2 \times 10^6$  viable cells were suspended in 0.2 ml PBS and injected retroorbitally in each group of mice. Five days after injection, the ATMs were isolated from visceral fat tissue and analyzed by FACS <sup>25</sup>.

### **Glucose uptake in primary adipocyte and 3T3-L1 adipocyte**

Glucose uptake in primary adipocyte and 3T3-L1 adipocyte were measured as previously described <sup>8,23</sup>.

### **Intraperitoneal primary macrophage isolation and culture**

We harvested primary macrophages from WT and Gpr120 KO mice as described <sup>8</sup>. Three days after harvest and plating, we pretreated cells with 100  $\mu$ M DHA or 10  $\mu$ M cpdA for 1 hr, followed by LPS (100 ng ml<sup>-1</sup>) for 15 min prior to protein isolation, 6 hr for collection of condition media and RNA isolation for qPCR analyses. For the NFkB-luc reporter assay was conducted as described <sup>26</sup> with primary macrophages from WT and Gpr120 KO mice.

### **Nitrate measurement**

Nitrate content in adipose tissue lysate was measured using Griess Reagent System (Promega) in accordance with the manufacturer's protocol.

### **Measurement of protein nitrosylation**

S-nitrosylation of Akt was detected using the biotin-switch method (Cayman) according to the manufacturer's protocol.

## Lipid measurement

Lipid measurements in mouse liver was performed by *Lipomics* as described previously<sup>8</sup>.

## LTB4 measurement

LTB4 measurement in mouse adipose tissue was performed as previously described<sup>27</sup>.

## Measurement of Insulin Secretory Response from Isolated Islets

Glucose-stimulate insulin secretion from mouse islet was performed as previously described<sup>28</sup>. For static GSIS assays, ~20 mouse islets were incubated for 2 hr in low glucose media at 37 °C, 5% CO<sub>2</sub>, and then incubated for 60 min or 75 min with 2.8 mM or 16.7 mM glucose in the same conditions.

## RNA library construction and High-throughput sequencing

RNA library construction and Illumina high-throughput sequencing was performed as described previously<sup>29</sup>.

## Processing RNA-seq data for information clustering and heatmap

RNA sequences from Illumina HiSeq were aligned to the mouse transcriptome using the *Bowtie2* aligner<sup>30</sup>. Gene-level count summaries were analyzed for statistically significant changes using *DESeq*<sup>31</sup>. Individual *p*-values were adjusted for multiple testing by calculating the *q*-values. For each gene, the *q*-value is the smallest false discovery rate at which the gene is found significant. For Information clustering and heatmap generation, We analyzed biological processes as defined by the Gene Ontology Consortium<sup>32</sup>. A typical list of significant biological processes usually contains several redundant, closely related gene sets with great overlap of member genes. In order to reduce redundancy of reporting, we cluster the significant terms using a true distance metric called variation of information<sup>33</sup>. Qualitatively speaking, variation of information between two sets of genes is smaller (i.e., gene sets are closer) when the gene sets share a large fraction of member genes and is larger (gene sets are farther apart) when the gene memberships have less overlap. A distance matrix thus obtained defines a graph in higher-dimensional Euclidean space in which each node is a gene set and the length of every edge is the distance (variation of information) between the connected nodes. This graph is then optimally visualized in two dimensions using a Principal Coordinates Analysis (multiscaling) function *cmdscale* of *R*. For presentation purposes, we choose to represent each node (gene set) not just by a point, but a circle whose diameter is proportional to the  $(-\log)$  of the Bonferroni-adjusted *P* value. This way, more significant nodes appear as larger circles to draw attention. Any two circles may appear to overlap, but this should not be interpreted in the usual Venn diagram sense. When circles overlap, it is because the gene sets they represent were close enough in the information sense (had overlapping gene membership) and was significant enough to produce large circles. We use this visualization to report the relevant non-redundant biological processes.

## Data analysis

Densitometric quantification and normalization were performed using the ImageJ 1.42q software. The values presented are expressed as the means $\pm$ SEM. The statistical significance of the differences between various treatments was determined by one-way ANOVA with the Bonferroni correction using GraphPad Prism 6.0 (San Diego, CA).  $p < 0.05$  was considered significant.

## Supplementary Material

Refer to Web version on PubMed Central for supplementary material.

## Acknowledgments

This study was funded in part by grants to J.M.O (DK033651, DK074868, DK063491, DK09062), and D.Y.O. (P30 DK063491), a grant from Merck Inc. to J.M.O. and D.Y.O., Austrian science fund (FWF Doktoratskolleg DK-MCD W1226 and the FWF project P24143) to J.G.B.S., and Marshall Plan Scholarship to A.R.P.

We thank Angela Tyler for editorial assistance and Neal Sekiya for assistance with FACS analysis at the VA San Diego hospital, the UCSD Histology Core lab for technical help with processing liver specimens, and the UCSD Microscope Resource for microscopy analysis which is funded by UCSD Neuroscience Microscopy Shared Facility Grant P30 NS047101.

## References

1. Sijben JW, Calder PC. Differential immunomodulation with long-chain n-3 PUFA in health and chronic disease. *Proc Nutr Soc.* 2007; 66:237–259. [PubMed: 17466105]
2. Lee JY, et al. Differential modulation of Toll-like receptors by fatty acids: preferential inhibition by n-3 polyunsaturated fatty acids. *J Lipid Res.* 2003; 44:479–486. [PubMed: 12562875]
3. Proudman SM, Cleland LG, James MJ. Dietary omega-3 fats for treatment of inflammatory joint disease: efficacy and utility. *Rheum Dis Clin North Am.* 2008; 34:469–479. [PubMed: 18638687]
4. Calder PC. Polyunsaturated fatty acids and inflammation. *Biochem Soc Trans.* 2005; 33:423–427. [PubMed: 15787620]
5. Polozova A, Salem N Jr. Role of liver and plasma lipoproteins in selective transport of n-3 fatty acids to tissues: a comparative study of 14C-DHA and 3H-oleic acid tracers. *J Mol Neurosci.* 2007; 33:56–66. [PubMed: 17901547]
6. Neschen S, et al. n-3 Fatty acids preserve insulin sensitivity in vivo in a peroxisome proliferator-activated receptor- $\alpha$ -dependent manner. *Diabetes.* 2007; 56:1034–1041. [PubMed: 17251275]
7. Geleijnse JM, Giltay EJ, Grobbee DE, Donders AR, Kok FJ. Blood pressure response to fish oil supplementation: meta-regression analysis of randomized trials. *J Hypertens.* 2002; 20:1493–1499. [PubMed: 12172309]
8. Oh DY, et al. GPR120 is an omega-3 fatty acid receptor mediating potent anti-inflammatory and insulin-sensitizing effects. *Cell.* 2010; 142:687–698. [PubMed: 20813258]
9. Ichimura A, et al. Dysfunction of lipid sensor GPR120 leads to obesity in both mouse and human. *Nature.* 2012; 483:350–354. [PubMed: 22343897]
10. Itoh Y, et al. Free fatty acids regulate insulin secretion from pancreatic beta cells through GPR40. *Nature.* 2003; 422:173–176. [PubMed: 12629551]
11. Hudson BD, et al. The pharmacology of TUG-891, a potent and selective agonist of the free fatty acid receptor 4 (FFA4/GPR120), demonstrates both potential opportunity and possible challenges to therapeutic agonism. *Molecular pharmacology.* 2013; 84:710–725. [PubMed: 23979972]
12. Hirasawa A, et al. Free fatty acids regulate gut incretin glucagon-like peptide-1 secretion through GPR120. *Nature medicine.* 2005; 11:90–94.
13. Hara T, et al. Novel selective ligands for free fatty acid receptors GPR120 and GPR40. *Naunyn-Schmiedeberg's archives of pharmacology.* 2009; 380:247–255.

14. Shimpukade B, Hudson BD, Hovgaard CK, Milligan G, Ulven T. Discovery of a potent and selective GPR120 agonist. *Journal of medicinal chemistry*. 2012; 55:4511–4515. [PubMed: 22519963]
15. Sun Q, et al. Structure-activity relationships of GPR120 agonists based on a docking simulation. *Molecular pharmacology*. 2010; 78:804–810. [PubMed: 20685848]
16. Paulsen SJ, et al. Expression of the fatty acid receptor GPR120 in the gut of diet-induced-obese rats and its role in GLP-1 secretion. *PloS one*. 2014; 9:e88227. [PubMed: 24520357]
17. Xiong Y, et al. Activation of FFA1 mediates GLP-1 secretion in mice. Evidence for allosterism at FFA1. *Molecular and cellular endocrinology*. 2013; 369:119–129. [PubMed: 23403053]
18. Stone VM, et al. GPR120 (FFAR4) is preferentially expressed in pancreatic delta cells and regulates somatostatin secretion from murine islets of Langerhans. *Diabetologia*. 2014
19. Feuerer M, et al. Lean, but not obese, fat is enriched for a unique population of regulatory T cells that affect metabolic parameters. *Nature medicine*. 2009; 15:930–939.
20. Nishimura S, et al. Adipose Natural Regulatory B Cells Negatively Control Adipose Tissue Inflammation. *Cell metabolism*. 2013
21. Yasukawa T, et al. S-nitrosylation-dependent inactivation of Akt/protein kinase B in insulin resistance. *The Journal of biological chemistry*. 2005; 280:7511–7518. [PubMed: 15632167]
22. Li P, et al. Adipocyte NCoR knockout decreases PPARgamma phosphorylation and enhances PPARgamma activity and insulin sensitivity. *Cell*. 2011; 147:815–826. [PubMed: 22078880]
23. Talukdar S, et al. Neutrophils mediate insulin resistance in mice fed a high-fat diet through secreted elastase. *Nature medicine*. 2012; 18:1407–1412.
24. Li P, et al. Functional heterogeneity of CD11c-positive adipose tissue macrophages in diet-induced obese mice. *The Journal of biological chemistry*. 2010; 285:15333–15345. [PubMed: 20308074]
25. Oh DY, Morinaga H, Talukdar S, Bae EJ, Olefsky JM. Increased macrophage migration into adipose tissue in obese mice. *Diabetes*. 2012; 61:346–354. [PubMed: 22190646]
26. Li P, et al. NCoR repression of LXRs restricts macrophage biosynthesis of insulin-sensitizing omega 3 fatty acids. *Cell*. 2013; 155:200–214. [PubMed: 24074869]
27. Quehenberger O, et al. Lipidomics reveals a remarkable diversity of lipids in human plasma. *J Lipid Res*. 2010; 51:3299–3305. [PubMed: 20671299]
28. Lee YS, et al. The fractalkine/CX3CR1 system regulates beta cell function and insulin secretion. *Cell*. 2013; 153:413–425. [PubMed: 23582329]
29. Lister R, et al. Hotspots of aberrant epigenomic reprogramming in human induced pluripotent stem cells. *Nature*. 2011; 471:68–73. [PubMed: 21289626]
30. Langmead B, Salzberg SL. Fast gapped-read alignment with Bowtie 2. *Nature methods*. 2012; 9:357–359. [PubMed: 22388286]
31. Anders S, Huber W. Differential expression analysis for sequence count data. *Genome biology*. 2010; 11:R106. [PubMed: 20979621]
32. Reference Genome Group of the Gene Ontology, C. The Gene Ontology's Reference Genome Project: a unified framework for functional annotation across species. *PLoS computational biology*. 2009; 5:e1000431. [PubMed: 19578431]
33. Nugent R, Meila M. An overview of clustering applied to molecular biology. *Methods in molecular biology*. 2010; 620:369–404. [PubMed: 20652512]

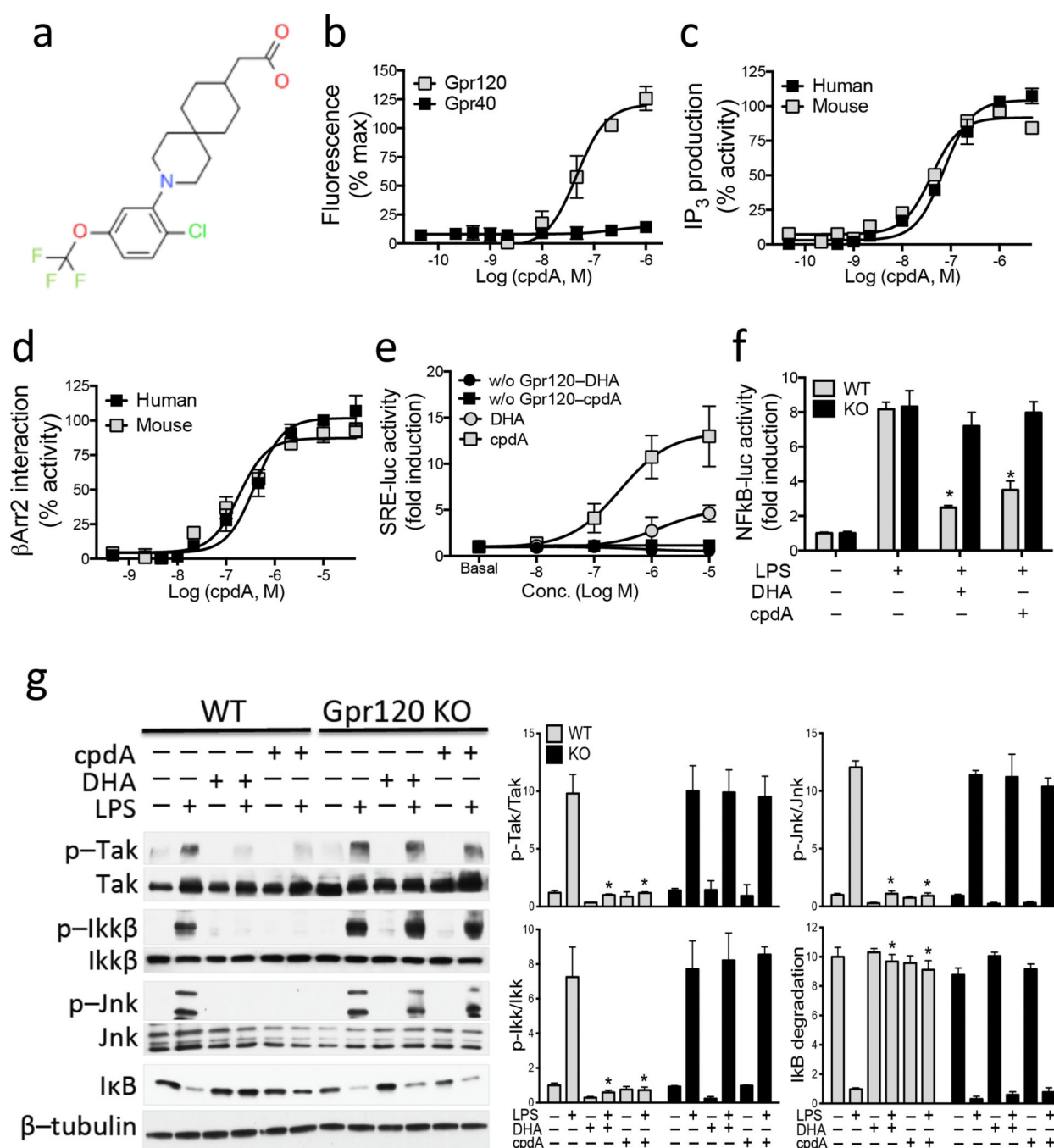


**Figure 1. CpdA is a selective agonist of Gpr120**

(a) Chemical structure of cpdA. Dose response data for cpdA are shown in (b)  $\text{Ca}^{2+}$  mobilization for Gpr120 vs. Gpr40 transfected cells. Dose response data for cpdA are shown in (c)  $\text{IP}_3$  production, and (d)  $\beta$ -arrestin-2 interaction assay with human and mouse Gpr120. Results are % activity over basal. (e) Gpr120-mediated SRE-luc activity after treatment with DHA and cpdA for 6 hr in HEK 293 cells. (f) NFkB-luc activity after pretreatment with DHA and cpdA for 1 hr subjected followed by LPS for 6 hr in primary macrophages from WT or Gpr120 KO mice. Results are fold activities over basal. Each data point represents

mean $\pm$ SEM of three independent experiments performed in triplicate.  $P<0.05$  versus LPS treatment in WT macrophages. **(g)** DHA and cpdA inhibits LPS-induced inflammatory signaling in primary macrophages from WT, but not Gpr120 KO macrophages. The scanned bar graph (right panel) shows fold induction over basal conditions (p-Tak, p-Ikk, and p-Jnk) or LPS treatment (IkB degradation). Data are expressed as the mean $\pm$ SEM. \*,  $P<0.05$  versus LPS treatment in WT mice to DHA+LPS or cpdA+LPS.  $n=6$  per group. Data is a representative image from more than five independent experiments.

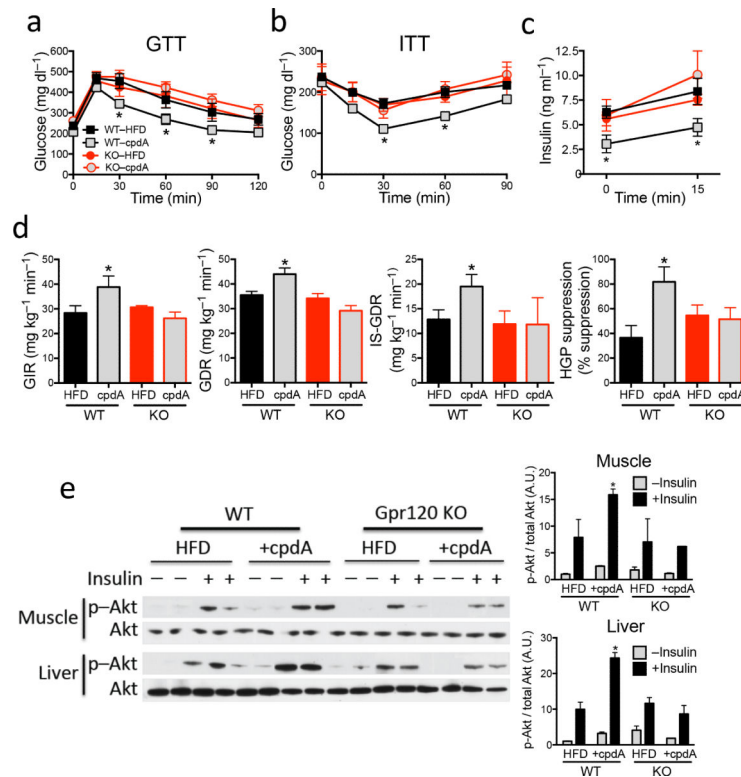


**Figure 2. Gpr120 agonist and *in vivo* metabolic studies**

(a) GTT in WT and Gpr120 KO mice on HFD or HFD+cpdA. *n*=10 per group. (b) ITT in WT and Gpr120 KO mice on HFD or HFD+cpdA. *n*=10 per group. (c) Plasma insulin level during GTT at the indicated time points. (d) Hyperinsulinemic/euglycemic clamp studies in WT and Gpr120 KO mice on HFD or HFD+cpdA. Glucose infusion rate (GIR), total glucose disposal rate (GDR), insulin-stimulated glucose disposal rate (IS-GDR), percent suppression of hepatic glucose production. \*, *p*<0.05, compared to HFD. Data are represented as mean±SEM. (e) Acute insulin response showing phosphorylation of Akt in skeletal muscle and liver from WT and Gpr120 KO mice on HFD or HFD+cpdA using 0.35 U kg<sup>-1</sup> insulin injected via inferior vena cava. Left panel is a representative image from five independent experiments, and the scanned bar graph (right panel) shows fold induction over basal (before insulin injection) conditions. Data are expressed as the mean±SEM. \*, *P*<0.05 versus insulin injection in WT mice on HFD. *n*=6 per group.

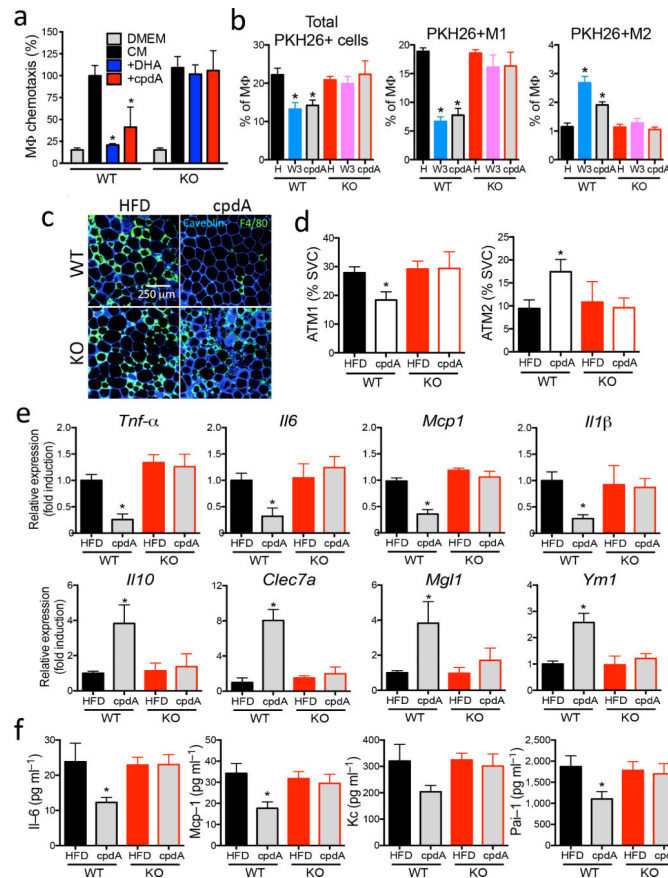


**Figure 3. Anti-inflammatory effects of Gpr120 agonism**

(a) Effect of Gpr120 agonist on 3T3-L1 adipocyte CM-induced chemotaxis of primary macrophage from WT and Gpr120 KO mice. (b) *In vivo* tracking of PKH26 positive monocytes in WT and Gpr120 KO mice on HFD or HFD+ω3-FA (W3) or HFD+cpdA. *n*=6 per group. (c) ATM content by F4/80 staining in adipose tissue sections from WT and Gpr120 KO mice on HFD or HFD+cpdA. Scale bar indicates 250 μm. (d) FACS analysis of ATMs from WT and Gpr120 KO mice on HFD or HFD+cpdA. *n*=6 per group. (e) Relative mRNA level of inflammatory cytokines (upper row) and anti-inflammatory cytokines (lower row) in adipose tissue from WT and Gpr120 KO mice from HFD or HFD+cpdA. *n*= 10 per group. (f) Serum Il-6, Mcp-1, Kc, and Pai-1 levels from WT and Gpr120 KO mice on HFD or HFD+cpdA. *n*= 10 per group. Data are expressed as the mean±SEM. \*, *P*<0.05 versus WT mice on HFD.

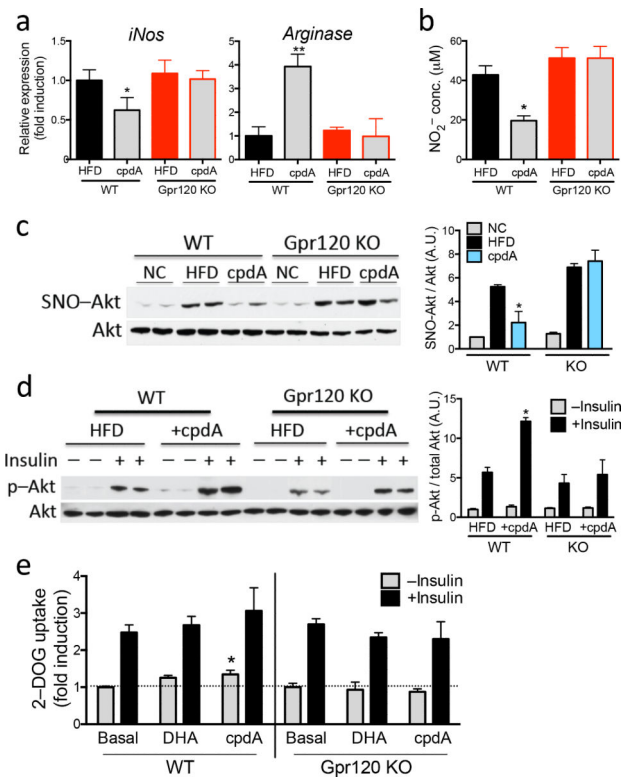


**Figure 4. Production of NO and glucose uptake in adipocytes**

(a) mRNA levels of *iNos* and *Arginase* in adipose tissue from WT and Gpr120 KO mice on HFD or HFD+cpdA.  $n=10$  per group. (b) Nitric oxide level in adipose tissue of WT and Gpr120 KO mice on HFD or HFD+cpdA.  $n=8$  per group. (c) HFD-induced nitrosylation of Akt in adipose tissue is reduced only in WT on HFD+cpdA. (d) Akt phosphorylation in adipose tissue from WT or Gpr120 KO mice on HFD or HFD+cpdA before and after insulin injection. Left panel is a representative image from three independent experiments, and the scanned bar graph (right panel) shows fold induction over basal. Data are expressed as the mean $\pm$ SEM. \*,  $p<0.05$  versus insulin injection in WT mice on HFD.  $n=6$  per group. (e) Glucose uptake in primary adipocytes from WT and Gpr120 KO mice and pretreated with DHA or cpdA for 30 min and subsequently incubated in the absence and presence of insulin, followed by measurement of 2-deoxyglucose (2-DOG) uptake. Data are expressed as the mean $\pm$ SEM from three independent experiments. \* indicates significance at  $P<0.05$  over basal.